ACCOUNTS
of chemical research

Electron Holography for the Study of Magnetic Nanomaterials

JOHN MEURIG THOMAS,*,† EDWARD T. SIMPSON,†
TAKESHI KASAMA,† AND RAFAL E. DUNIN-BORKOWSKI†,‡

†Department of Materials Science and Metallurgy, University of Cambridge, Pembroke Street, Cambridge CB2 3QZ, U.K., and ‡Center for Electron Nanoscopy, Technical University of Denmark, DK-2800 Kongens Lyngby, Denmark

RECEIVED ON OCTOBER 15, 2007

CONSPECTUS

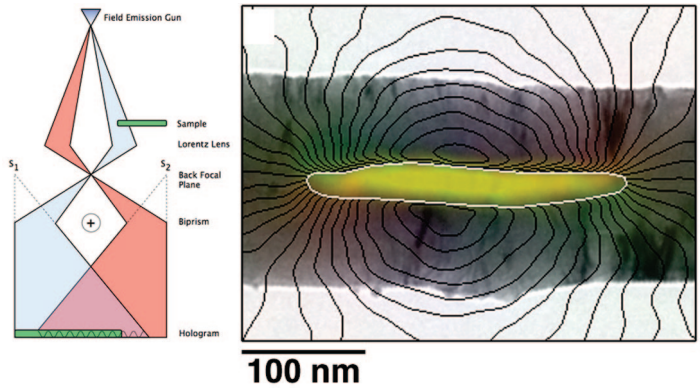

Transmission electron microscopes fitted with field-emission guns (to provide coherent electron waves) can be adapted to record the magnetic fields within and surrounding nanoparticles or metal clusters, for example, the lines of force of a nanoferromagnet encapsulated within a multiwalled carbon nanotube. Whereas most chemists are aware that electron microscopy readily identifies crystallographic symmetries and phases, solves structures, and, in conjunction with electron energy-loss spectroscopy, yields valence states and electronic information of materials, relatively few know that it can also provide important quantitative information, with nanometer-scale spatial resolution, pertaining to such materials' magnetic properties. In this Account, with the aid of representative examples embracing solid-state chemistry, geochemistry, and bio-inorganic phenomena, we illustrate how off-axis electron holography affords deep insight into magnetic phenomena on the nanoscale. Specifically, we describe the unprecedented level of information available regarding the magnetic nature of magnetotactic bacteria, magnetic nanoparticle chains and chiral bracelets, and geochemically relevant phenomena involving exsolution (the un-mixing of two mineral phases, as in the magnetite−ulvöspinel system). It is, for example, possible to reveal vortices and multidomain states that have no net magnetization in minute blocks of magnetite.

With the current burgeoning interest and activity in nanoscience and nanotechnology, our Account concludes with examples of some existing enigmas that electron holography, especially when augmented by the related technique of electron tomography, might play an important experimental role in resolving, such as the occurrence of ferromagnetism in nanocrystals of silver within carbon tubes and in clusters of alkali metals incarcerated within zeolites.

1. Introduction

In 1831, the founding father of magnetochemistry (and of field theory), Michael Faraday, pondered the nature of magnetic lines of force and illustrated their existence by sprinkling iron filings on to a sheet of paper, beneath which he placed one or more permanent magnets. One of the actual patterns generated by Faraday and "fixed" by him[1] is shown in Figure 1a. A more recent example of a similar pattern obtained from a single bar magnet is shown in Figure 1b. Faraday's

Published on the Web 05/07/2008 www.pubs.acs.org/acr
10.1021/ar700225v CCC: $40.75 © 2008 American Chemical Society

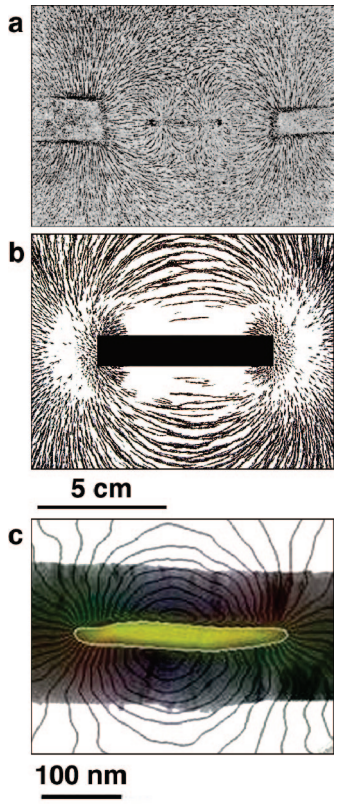

FIGURE 1. (a) Michael Faraday's image of "magnetic lines of force", formed using magnets and iron filings (this image is shown in Figure 24 on p 47 of ref 1), (b) a contemporary image similar to that shown in panel a formed using a single bar magnet and iron filings, and (c) magnetic phase contours recorded using off-axis electron holography from a multiwalled carbon nanotube, approximately 180 nm in diameter, containing a 36-nm-diameter encapsulated iron crystal (in yellow). The contours, which were generated from the phase image, were overlaid onto a bright-field TEM image of the crystal.[4]

experimental work prompted Maxwell to interpret lines and tubes of force in a landmark paper[2] on electromagnetism in 1856, an achievement that was to change the intellectual framework of physics. Although the notion of lines of force has subsequently been modified, the term is still used extensively; see, for example, Tonomura's work[3] on the reconstruction of magnetic fields using off-axis electron holography. The technique of electron holography, which is the subject of this Account, can be used strikingly to demonstrate the nature of magnetic vector fields, as may be seen in Figure 1c, which shows the experimentally measured magnetic field of a minute ferromagnetic crystal of iron encapsulated in a multiwalled carbon nanotube,[4] a nanoscale analogue of the pattern shown in Figure 1b.

The principal aim of the present Account is to describe how such fields may be "captured" and to discuss the future potential of electron holography in the chemical sciences and nanotechnology.[5] A powerful complimentary technique, electron tomography, which can be used to yield three-dimensional information about the shapes and sizes of materials with subnanometer resolution, is mentioned briefly herein and described in detail elsewhere.[6]

Although the word holography is nowadays popularly associated with the three-dimensional reconstruction of objects via coherent (laser) light of appropriate 2D photographs, the technique itself, proposed by Gabor,[7] has its origins rooted firmly in electron microscopy. Electron holography is based on the formation of an interference fringe pattern or "hologram" in a transmission electron microscope (TEM). In contrast to most conventional TEM techniques, which are used to record only the spatial distribution of image intensity, electron holography also allows the phase shift of the high-energy electron wave that has passed through the specimen to be measured. The recorded phase shift can be used to yield information about local variations in magnetic induction and electrostatic potential in and around the specimen. It is possible, as shown below, to separate these two contributions to the phase shift. Here, we focus exclusively on the retrieval of magnetic information from electron holograms, as the fields of nanoscience and nanotechnology are now replete with numerous new kinds of magnetochemical phenomena that may be suitable for detailed study using this technique. For example, more needs to be known about the local magnetic properties of colloidal nanocrystals of Fe,[8] Co,[9] and CoPt[10] and about colloidal ferrofluids and mixed-metal ferrites.[11] The observed exponential dependence of magnetization relaxation time on nanoparticle volume has stimulated studies of the synthesis of ferromagnetic nanoparticles for the purpose of magnetic storage, as well as new molecular and metal oxide magnets. Photoinduced magnetization in materials such as copper-octacyanomolybdate,[12] in addition to the phenomenon of humidity-induced magnetization and magnetic pole inversion in other cyano-bridged metal assemblies,[13] may also merit further investigation by some of the holographic procedures that we describe.

It should be stressed that examination of some of the systems described will be a significant challenge and would push holography toward its current limits. However, current and future development of the technique should bring holography to the point where these problems are soluble.

Recent studies using the "off-axis" mode of electron holography have already yielded unprecedented insights into the magnetic natures of magnetotactic bacteria[14] (see section 3.2), nanoparticle (magnetic) chains and chiral braceletes[15] (section 3.3) and geochemically relevant phenomena involving exsolution (the unmixing of two mineral phases), as we

describe for the magnetite–ulvöspinel system[16] in section 3.4. The technique is capable of imaging magnetization states within individual magnetic particles, as well as magnetostatic interactions between neighboring particles. Contour lines placed on the magnetic contribution to the recorded phase shift (as illustrated in Figure 1c) can be used to provide quantitative images of lines of projected in-plane magnetic flux density with a spatial resolution approaching nanometers. Moreover, since electron holograms are recorded in a TEM, other analytical advantages prevail, including the ability to identify crystallographic phases (from selected area electron diffraction), compositions (from energy-dispersive X-ray emission or electron energy-loss spectroscopy),[17,18] and sizes and shapes (from electron tomography[6,18]).

2. Experimental Set-Up and Background Theory[19–21]

The off-axis[20,21] TEM mode of recording electron holograms involves the examination of an electron-transparent specimen using defocused illumination from a highly coherent field emission gun electron source. The region of interest is positioned so that it covers approximately half the field of view. The application of a voltage to an electron biprism results in overlap of a "reference" electron wave that has passed through vacuum with another part of the same electron wave that has passed through the specimen, as shown schematically in Figure 2a. If the electron source is sufficiently coherent, then, in addition to an image of the specimen, an interference fringe pattern is formed in the overlap region, as shown in Figure 2b. The amplitude and the phase shift of the electron wave that leaves the specimen are recorded in the intensity and the position, respectively, of the holographic interference fringes. For studies of magnetic materials, a Lorentz lens (a high-strength minilens) allows the microscope to be operated at high magnification with the objective lens switched off and the specimen located in magnetic-field-free conditions.

The recorded phase shift is sensitive both to the in-plane component of the magnetic induction and to the electrostatic potential in the specimen. If we assume that the specimen is weakly diffracting (i.e., ignoring dynamical contributions to the contrast) then the phase shift $\varphi(x)$ may be expressed in the form[18–21]

$$\varphi(x) = C_E \int V(x,z)\, dz - \left|\frac{e}{h}\right| \int\int B_\perp(x,z)\, dx\, dz \qquad (1)$$

where

$$C_E = \left(\frac{2\pi}{\lambda}\right)\left(\frac{E+E_0}{E(E+2E_0)}\right) \qquad (2)$$

z is the electron-beam direction, x is a direction in the plane of the specimen, $B_\perp$ is the component of the magnetic induction perpendicular to x and z, V is the electrostatic potential,

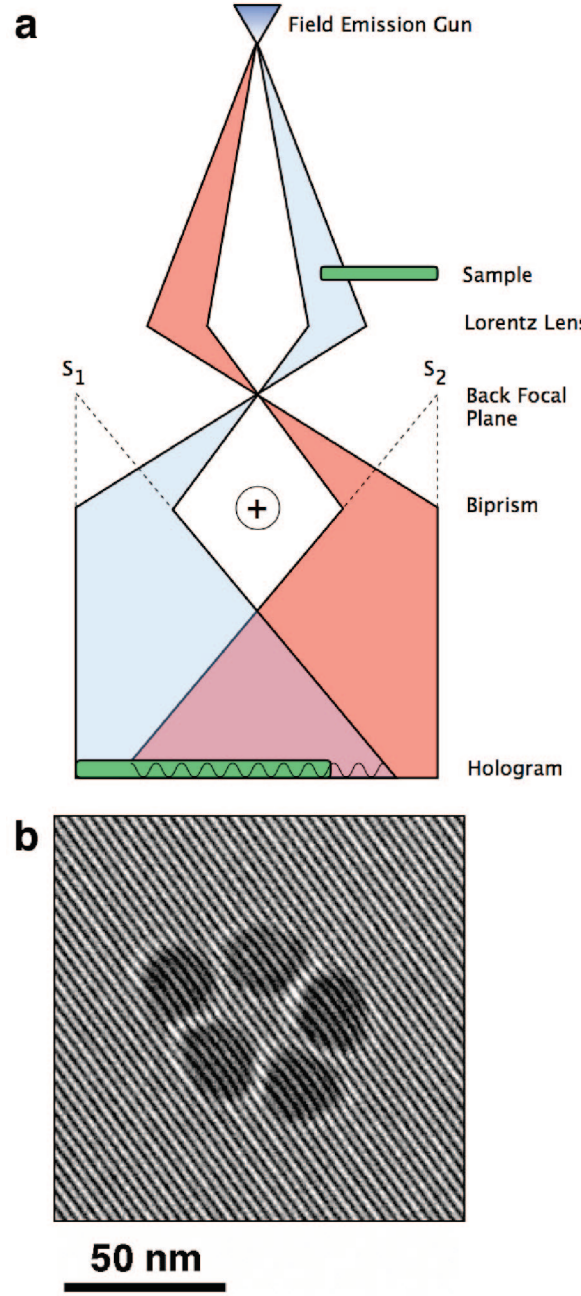

FIGURE 2. (a) Schematic diagram illustrating the application of a voltage to an electron biprism located close to a conjugate image plane in the microscope, in order to overlap a "reference" electron wave that has passed through vacuum with the electron wave that has passed through the specimen, to form an off-axis electron hologram and b representative off-axis electron hologram of five 20–30 nm cobalt nanoparticles obtained from the specimen described in Figure 5 below.

λ is the (relativistic) electron wavelength and E and E_0 are, respectively, the kinetic and rest mass energies of the incident electron. If neither V nor $B_\perp$ varies along the electron-beam direction in a specimen of thickness t, and in the absence of electrostatic or magnetic fringing fields outside the specimen, equation 1 can be simplified as

$$\varphi(x) = C_E V(x) t(x) - \left(\frac{e}{h}\right) \int B_\perp(x) t(x)\, dx \qquad (3)$$

By use of eqs 1−3, information about V and $B_\perp$ can be recovered from a measured phase image.

Recent applications of electron holography to the characterization of magnetic fields in nanostructured materials (e.g., ref 20) have almost invariably made use of digital recording. Of particular interest for magnetic materials is the digital determination of the gradient of the phase image. The phase gradient is directly proportional to the in-plane component of the magnetic induction in the specimen, and a graphical representation of the strength and direction of the local projected in-plane magnetic induction may be obtained simply by adding contours to the recorded magnetic contribution to the phase image.

A great advantage of the digital analysis of electron holograms is that the magnetic and mean inner potential contributions to the observed phase shift can often be separated readily. The most practical approach to this involves performing a magnetization reversal experiment *in situ* in the electron microscope by exciting the conventional objective lens, and subsequently selecting pairs of holograms that differ only in the (opposite) direction of magnetization in the specimen. The magnetic and mean inner potential contributions to the phase shift may be calculated by taking half the difference and half the sum of the resulting phase images, respectively.

3. Specific Examples

3.1. Isolated Magnetite Crystal. We begin, for heuristic purposes, by illustrating the application of off-axis electron holography to the characterization of an isolated 50-nm-diameter single crystal of magnetite (Fe_3O_4) from a bacterial cell.

Figure 3a[19] shows a high-resolution TEM image of the crystal. Figure 3b shows its three-dimensional morphology and orientation, determined by applying electron tomography[6] to a series of high-angle annular dark-field (HAADF) images taken over an ultrahigh range of specimen tilt angles. In the absence of significant shape anisotropy and interactions with neighboring crystals, a crystal's magnetic properties may be dominated by magnetocrystalline anisotropy, the magnitude and direction of which are known to change with temperature. Accordingly, magnetic induction maps were obtained from electron holograms of the crystal acquired in magnetic-field-free conditions both at room temperature (Figure 3c) and at 90 K (below the Verwey transition[22] for magnetite) (Figure 3d). Both panels c and d of Figure 3 show uniformly magnetized single-domain magnetic states, including the characteristic return flux of an isolated magnetic dipole.[23] Quantitative analysis of the room-temperature phase image indicates that the magnetization direction of the particle lies in the plane of the specimen, close to a ⟨111⟩ crystallographic direction and parallel to the longest diagonal dimension of the particle, consistent with shape anisotropy dominating the magnetic state of the crystal. Similar analysis of the recovered phase at 90 K suggests that, at remanence, the magnetization direction in the crystal is tilted out of the plane by ∼40° to the horizontal. This direction is close to a ⟨100⟩ direction in the original cubic crystal. Below the Verwey transition, the magnetocrystalline anisotropy of magnetite is known to increase in magnitude and to switch from $\langle 111 \rangle_{cubic}$ to $[001]_{monoclinic}$. The results confirm the prediction that, in the absence of shape anisotropy and interactions, magnetocrystalline anisotropy has a significant effect on the remanence direction at 90 K.

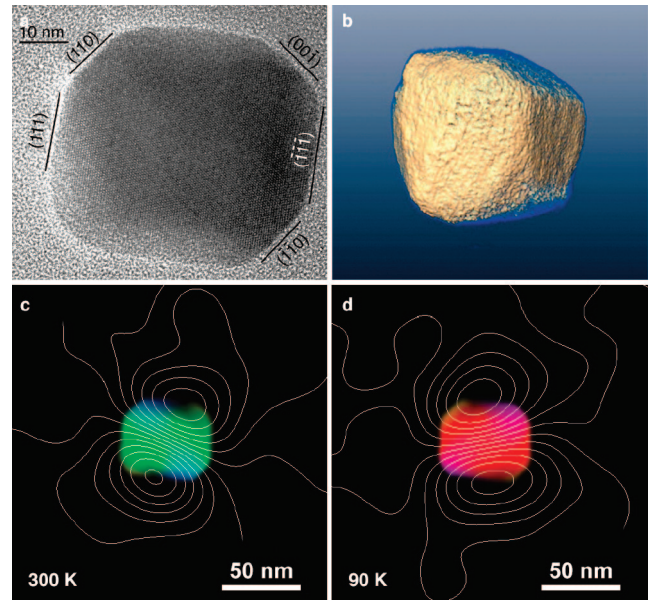

FIGURE 3. (a) High-resolution image of an isolated faceted 50-nm-diameter magnetite (Fe_3O_4) crystal from a magnetotactic bacterium on a holey carbon TEM grid, (b) isosurface visualisation of a high-angle annular dark-field tomographic reconstruction of the same particle, and (c, d) magnetic induction maps recorded using off-axis electron holography from the same particle, showing remanent magnetic states at room temperature and at 90 K, respectively.[24]

3.2. Magnetotactic Bacteria. Magnetotactic bacteria typically contain single or multiple chains of crystals of magne-

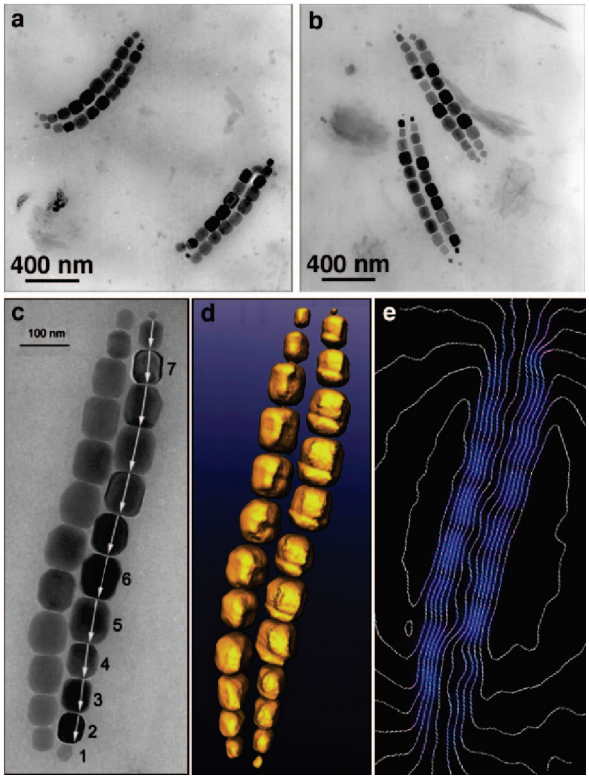

FIGURE 4. (a, b) Low-magnification bright-field images of magnetotactic bacteria that were air-dried onto carbon TEM grids. Each cell contains two pairs of double chains of magnetite (Fe_3O_4) crystals. (c) Bright-field TEM image of one double chain of magnetite crystals from a cell similar to those shown in panels a and b. The white arrows correspond to directions in the crystals that were identified as [111]. (d) Isosurface visualisation of a high-angle annular dark-field tomographic reconstruction of the double magnetosome chain shown in panel c. (e) Magnetic induction map recorded at room temperature using off-axis electron holography from the same double chain of magnetite crystals.[24a,b]

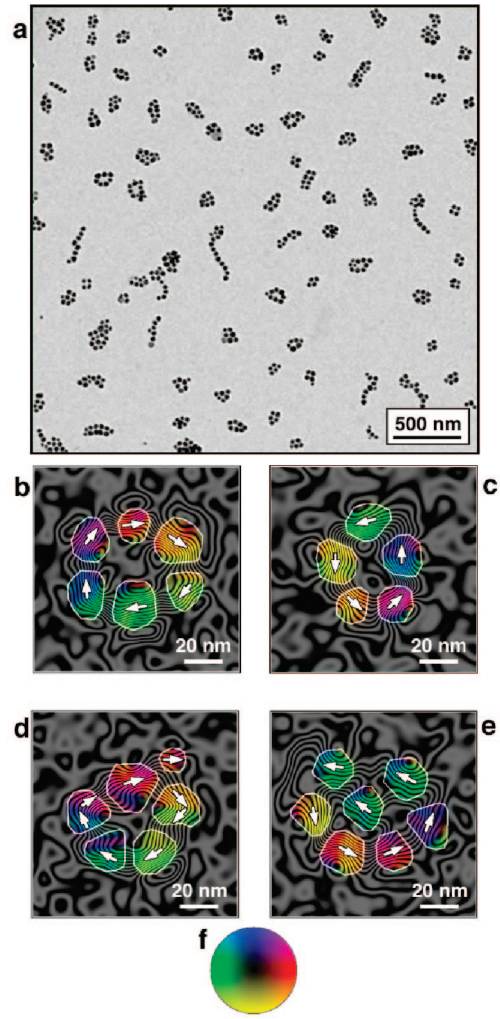

FIGURE 5. (a) Low-magnification bright-field image of self-assembled rings and chains of Co nanoparticles deposited directly onto a carbon TEM grid. Each particle has a diameter of between 20 and 30 nm. (b–e) Magnetic induction maps showing remanent states in four different Co nanoparticle rings, recorded using off-axis electron holography and displayed in the form of magnetic phase contours formed from the magnetic contribution to the measured phase shift. The outlines of the nanoparticles are marked in white, while the direction of the measured magnetic induction is indicated both using arrows and according to the color wheel shown in panel f.[27]

tite (Fe_3O_4) or greigite (Fe_3S_4) (see Figure 4a,b) that are between 35 and 120 nm in length. In this size range, the crystals are uniformly magnetized single magnetic domains at room temperature, and the arrangement of the crystals in linear chains results in a magnetic moment that orients the bacterial cell parallel to the geomagnetic field in an aquatic environment (thereby facilitating its search for a nutrient-rich environment).

Many of the physical attributes of bacterial magnetosomes have been discovered through the techniques of transmission electron microscopy:[24] their natures, sizes, and crystal structures, their strict alignment, their three-dimensional structures (from electron tomography), and their magnetic characteristics (from off-axis electron holography). Examples of such measurements are shown in Figures 4c–e for a double chain of magnetite crystals. The magnetic induction map shown in Figure 4e illustrates the highly optimized linear nature of the magnetic field lines associated with a linear chain of magnetite magnetosomes.

3.3. Chiral Magnetic Properties of Self-Assembled Cobalt Nanoparticle Rings. Whereas micrometer-sized rings may be prepared by rapidly evaporating metal films, recently it has been shown[25] that nanoparticles of cobalt, when dispersed in dilute solutions of the surfactant C-undecylcalix[4]resorcinarene (see Figure 2 of ref 27), can self-assemble into bracelet-like rings whose dimensions are below the limits of conventional lithography.[26] Such rings are expected to form "flux-closure" (FC) magnetic states, in which the indi-

vidual magnetic dipoles align into a closed circuit and result in a net magnetic moment of zero. These nanorings (or bracelets) are of interest for high-density information storage devices, as they could function as bistable states with minimal magnetic "cross-talk".

Off-axis electron holography can be used to reveal the magnetic induction associated with different distributions of self-assembled cobalt nanoparticles.[27] In particular, the handedness of magnetic domain structures in cobalt nanoparticle rings may be discerned readily, as shown in Figure 5b−e where panels b and d are seen to be of the opposite sense to panels c and e.

Based on electron holography observations, a statistical sampling of FC states indicates[26] an approximately 50:50 (i.e., racemic) mixture of clockwise and anticlockwise ground-state configurations, to which the rings relax after exposure to a saturating (2 T) out-of-plane magnetic field. It is significant that in the context of nanotechnological applications, such chiral FC states are stable at room temperature.

The formation of self-assembled aggregates (as seen in Figure 5a, in which chains and close-packed clusters of cobalt crystals are seen in addition to bracelets) illustrates the fundamental principles of colloid chemistry.[28]

3.4. Magnetic Interactions in Intergrowths of Ulvöspinel and Magnetite. Ulvöspinel (Fe_2TiO_4), which takes its name from the Ulvö islands of northern Sweden,[29] is a common component of titaniferous magnetite iron ores that occurs widely on Earth. Although the magnetite−ulvöspinel system forms a complete solid solution[16] at temperatures above about 450 °C, intermediate bulk compositions can exsolve during slow cooling to yield an intergrowth of single domain or pseudo-single-domain magnetite-rich blocks separated by nonmagnetic ulvöspinel-rich lamellae.

Harrison et al.[30] used off-axis electron holography to elucidate the magnetic microstructure of a natural finely exsolved intergrowth of submicrometer magnetite blocks in an ulvöspinel matrix. Some of their key observations are reproduced in Figure 6. Figure 6a shows a chemical map (derived from energy-filtered imaging) of a representative area of the sample. Ulvöspinel-rich exsolution lamellae (red) subdivide the original titaniferous grain into an array of magnetite-rich blocks (blue). The profiles in Figure 6b,c, which were obtained from the line marked with a short white arrow in Figure 6a, show that little Ti is present in the blocks—they are essentially pure magnetite. Harrison et al.[30] used off-axis electron holography to show that the individual blocks of magnetite contain primarily single domain states. They also revealed the magnetostatic interaction fields between them, as illustrated in Figure 6d,e. These images illustrate the complexity of the magnetic structure of this system: it is dominated by the shapes of the blocks and by magnetostatic interactions. Magnetic superstates, in which clusters of magnetite blocks act collectively to form vortex and multidomain states that have zero net magnetization, are also visible in Figure 6d,e.

It has long been known[31] that the microstructures of minerals are petrogenetic indicators. The remanent magnetization is used by geophysicists to map the motions of continents and ocean beds resulting from the dynamics of plate tectonics. Electron holography has considerable potential in the field of measuring both remanent magnetizations and magnetization reversal mechanisms in rocks and for understanding mineral magnetism at the nanometer scale in general.[32]

3.5. Ferromagnetic Crystals Encapsulated in Carbon Nanotubes. Jourdain et al.[33] recently used off-axis electron holography to study periodic inclusions of ferromagnetic metal phosphide nanoparticles inside carbon nanotubes (Figure 7a), which were grown by sequential catalytic growth to encapsulate iron, the binary alloy iron−nickel, and the ternary alloy iron−cobalt−phosphorus as (catalyst) nanoparticles along the lengths of multiwalled carbon nanotubes. Off-axis electron holography was used to show that encapsulated Fe−Co−P nanoparticles as small as 20 nm in size are ferromagnetic at room temperature (Figure 7b−d), in accordance with the expected magnetic properties of bulk metal phosphides of the same structure and composition.

4. Concluding Remarks: A Brief Outline of Some Current Chemical Phenomena Worthy of Holographic Study and Developments of the Technique

4.1. Detection Limits and Future Studies. The detection limits, precision, accuracy, and spatial resolution of the magnetic signals that can be measured using electron holography have been discussed by de Ruijter and Weiss,[34] who suggested that a practical phase precision of $\pi/100$ radians may be achieved for a spatial resolution of 1−3 nm.[34] In material terms, this criterion corresponds to a detectable signal from a 3 nm particle with a remanent magnetization similar to that of magnetite, equivalent to approximately 800 μ_B.

Given that electron holography has the ability to yield quantitative and local information about nanoscale magnetic properties in a highly spatially resolved manner, supplemented by other information pertaining to chemical composition, valence state, and atomic structure, there is considerable scope for it to be applied to a variety of other

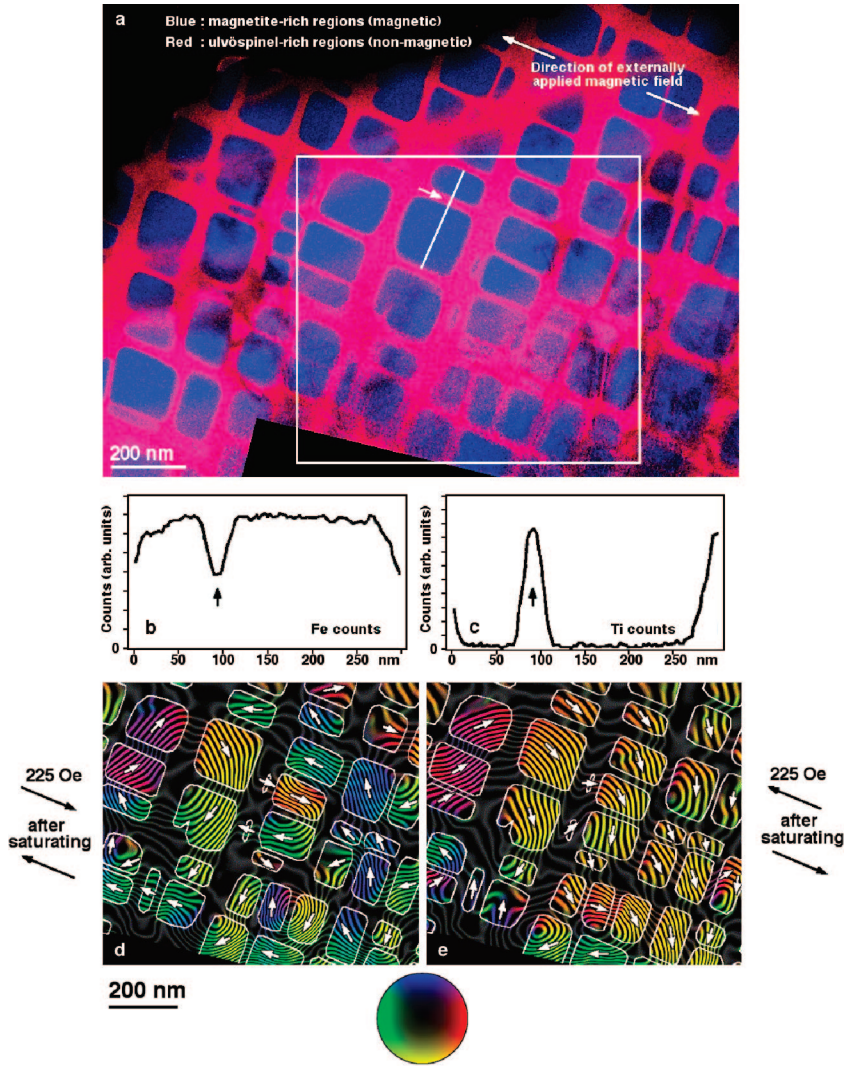

FIGURE 6. (a) Chemical map of an exsolved titanomagnetite (Fe_3O_4−Fe_2TiO_4) sample obtained using elemental mapping at the Fe $L_{2,3}$ and Ti $L_{2,3}$ edges in a Gatan imaging filter (GIF). The GIF separates electrons that have lost energy in the sample due to inelastic scattering from elastically scattered electrons and refocuses them to form an image of the sample. The blue regions are magnetic and are rich in magnetite (Fe_3O_4), while the red regions are nonmagnetic and rich in ulvöspinel (Fe_2TiO_4). The box corresponds to the region examined in detail using off-axis electron holography. Panels b and c show line profiles obtained from the Fe and Ti chemical maps, respectively, along the solid line marked in panel a. The short arrows mark the same point in the three pictures. (d, e) Magnetic microstructure of the boxed region in panel a measured using off-axis electron holography. The two images correspond to different magnetic remanent states, acquired with the sample in magnetic-field-free conditions.[30]

chemical problems.[35] Perspectives on possible problems that could be tackled in the future are now outlined.

4.1.1. Ferromagnetism Exhibited by Certain Encapsulated Nanoparticles of Metal. It is well-known[36] that cationic clusters of alkali metals such as Na_4^{3+} and K_3^{2+} are stable when "dissolved" within the cavities of microporous hosts such as zeolite Y. When Nozue et al.[37] reported that clusters of potassium bound inside certain zeolitic hosts exhibit ferromagnetism, it was greeted with surprise. The cause of this behavior and why the loaded zeolite exhibits spin-glass behavior remains enigmatic. It would be timely if a detailed electron holographic study were undertaken to establish the onset of ferromagnetism as a function of uptake of the alkali metal. Similarly, the recent report by Caudillo et al.[38] that nanocomposites consisting of minute particles of silver encapsulated in carbon nanospheres (∼10 nm diameter) show weak ferromagnetic behavior up to at least room temperature could benefit from an electron holography study to help clarify the physicochemical factors responsible for this. However, the sensitivity of the technique would require improvement beyond current levels to allow such a study to be worthwhile since such small signals are involved here. Future development of electron holography will therefore open doors to such studies.

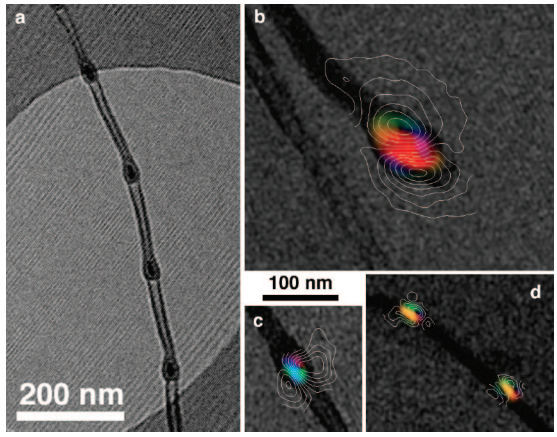

FIGURE 7. (a) Off-axis electron hologram recorded from a multiwalled carbon nanotube containing four periodically spaced Fe−Co−P crystals and (b−d) magnetic induction maps recorded using electron holography from crystals similar to those shown in panel a and overlaid onto amplitude images: (b) 52 nm × 98 nm particle; (c) 40 nm × 16 nm particle; (d) two particles in a nanotube.[33]

4.1.2. The Ferromagnetism of Dilute Magnetic Oxides. One of the most surprising discoveries in the field of magnetism has been that nonmagnetic semiconductors and insulators such as GaAs, ZnO, and TiO_2 become ferromagnetic at and above room temperature when they are doped with transition metal cations such as V, Cr, Mn, Fe, Co, or Ni.[39] This magnetism, which appears well below the cation percolation threshold,[40] cannot be understood in terms of the conventional theory of magnetism in insulators. Even more startling are claims that undoped films of these oxides are ferromagnetic or that they can become magnetic when doped with nonmagnetic cations. This has prompted Coey[41] to coin the term "d^0 ferromagnetism". Fresh insights into the root cause of these phenomena could be provided by the application of low-temperature electron holography, to enable detection of such weak signals.

4.1.3. The Materials Chemistry of Self-Assembled Nanocrystals. As described in section 3.3, inorganic colloids may nowadays be prepared in various self-assembled forms. It is also possible to modify the precise shapes of colloidal nanoparticles (from spheres to disks to rods and, more recently, to tetrapods[42]). There is little doubt that such self-assembled nanocrystals offer great potential for creating materials with an interesting confluence of mechanical, magnetic, optical, and electrical properties. Hardly anything is known experimentally about the manner in which the shapes of the individual nanocrystals that constitute such assemblies dictate their nanomagnetic properties, something holography could address.

4.1.4. Magnetic Nanoparticles and Heterogeneous Catalysis. A highly stable magnetically recoverable Pd catalyst[43] that is reusable for hydrogenation reactions can be prepared by the immobilization of Pd on silica-coated superparamagnetic magnetite nanoparticles. The catalyst nanoparticles are spatially well distributed over the magnetizable support surface, and they can be used to convert cyclohexene to cyclohexane very efficiently under mild conditions. The catalyst itself is readily recoverable with a permanent magnet in the reactor wall and is reusable up to some 20 times. It would be easy to extend this strategy to a variety of high-performance bimetallic nanoparticle catalysts (such as Pd_6Ru_6, $Pt_{10}Ru_2$, and Ru_6Sn[44]). Substantial practical improvements could be envisaged if more were known (from electron holography) about the magnetic properties of the silica-coated magnetite supports that are used, often under solvent-free and otherwise mild conditions.

4.2. Prospects for Improving Time Resolution in Electron Holography. In view of the many advantages that accrue from time-resolved electron microscopy in general (see the work of P. L. Gai et al.[45] and A. H. Zewail et al.[46]) it is both possible and timely to consider incorporating and improving the temporal dimension in electron holographic measurements. A real-time approach has been demonstrated by transferring electron holograms at TV rate onto a liquid-crystal spatial light modulator located at the output of a Mach−Zender interferometer.[47] More recently, an all-digital system that allowed reconstructed phase images to be displayed at approximately one frame per second has been facilitated by developments in computer speed.[48]

An example of where time-resolved electron holography would be illuminating occurs in the rapidly growing field of spintronics, where it becomes necessary to be able to follow the interplay between transient and permanent radicals and their role in governing the photomagnetic properties of various molecular devices.[49]

4.3. Prospects for Magnetic Vector Field Tomography. One of the major limitations of electron holography, as described so far, is that it is able only to image the *projection* of the in-plane magnetic field in the two-dimensional sample plane. However, by combining the already complimentary techniques of electron holography and electron tomography,[6] the three-dimensional magnetic vector field may be recoverable using suitable reconstruction techniques applied to two or four tilt series of electron holograms. The magnetic phase gradient of a sample (easily recoverable using electron holography) satisfies the projection requirement for electron tomographic reconstruction of one component of the magnetic

induction in three dimensions in the same way that material or chemical properties do, and this is currently being exploited to develop the technique and take nanomagnetic imaging into the third dimension.

The authors are grateful to Ryan K. K. Chong, Joshua M. Feinberg, Richard J. Harrison, Vincent Jourdain, Krzysztof Koziol, Mihály Pósfai, Andrew Putnis, Etienne Snoeck, Stephen L. Tripp, Alexander Wei, and Alan H. Windle for their valuable contributions and co-operation and to the Royal Society and the E.P.S.R.C. for financial support.

BIOGRAPHICAL INFORMATION

John Meurig Thomas, currently honorary professor of solid-state chemisty, Cambridge, was educated in the University of Wales and for 20 years taught and researched there before becoming Head of Physical Chemistry at Cambridge [1978−1986]. He was Director of the Royal institution of GB from 1986 to 1991. The recipient of numerous prizes, honorary doctorates, and Foreign Fellowships of many universities and academies for his work in solid-state, materials, and surface chemistry, he has pioneered the use and chemical applications of many facets of electron microscopy and spectroscopy since the mid-1960s. He is also renowned for his work on the design and characterization of nanoporous solids, which he has exploited to devise strategic principles for the production of a range of of single-site solid catalysts, especially for clean technology.

Edward Simpson was born in Shrewsbury, Shropshire, in 1981. He studied Experimental and Theoretical Physics in the University of Cambridge for his undergraduate and masters degrees, and completed his doctoral thesis at the department of Materials Science and Metallurgy in Cambridge on electron holography of nanomagnetic systems in early 2008. He was a Senior Scholar and Graduate President of Fitzwilliam College Cambridge and published a number of peer-reviewed papers during his Ph.D. research. Since January 2008, Ed has been an Associate at L.E.K. Consulting LLP in Belgravia, London.

Takeshi Kasama was born in Japan in 1974. He is currently a postdoctoral researcher in the Department of Materials Science and Metallurgy, University of Cambridge, studying the magnetic properties of minerals using electron holography. His Ph.D. was carried out in the Department of Earth and Planetary Science, University of Tokyo. After obtaining his degree, he was employed as a postdoctoral research scientist at the National Institute for Materials Science in Japan, at the University of Muenster in Germany, and at RIKEN (The Institute of Physical and Chemical Research) in Japan. While employed at RIKEN, he was also a long-term visitor at Cambridge. He has published over 50 peer-reviewed papers.

Rafal Dunin-Borkowski was born in London in 1969. He is presently Director of the newly established Center for Electron Nanoscopy in the Technical University of Denmark. He has conducted research on advanced TEM of nanoscale materials and devices for 17 years. He obtained his first degree in physics and Ph.D. from Cambridge University. He was subsequently a research associate in Cambridge University and Arizona State University and a senior research officer in Oxford University. Most recently, he held a Royal Society University Research Fellowship in the Department of Materials Science and Metallurgy in Cambridge, working on electron holography. He has published over 90 refereed journal papers and 14 book chapters.

FOOTNOTES

*To whom correspondence should be addressed. E-mail: jmt2@cam.ac.uk.

REFERENCES

1 Thomas, J. M. *Michael Faraday and the Royal Institution: The Genius of Man and Place*; Institute of Physics: Bristol, U.K., 1991.

2 Maxwell, J. C. On Faraday's lines of force. *Trans. Cambridge Philos. Soc.* **1856**, 10.

3 Tonomura, A. *The Quantum World Unveiled by Electron Waves*; World Scientific: Singapore, 1998.

4 Koziol, K.; Kasama, T.; Dunin-Borkowski, R. E.; Barpanda, P.; Windle, A. H. Electron holography of ferromagnetic nanoparticles encapsulated in three-dimensional arrays of aligned carbon nanotubes. *Mater. Res. Soc. Symp. Proc.* **2006**, *962E*, P13.03.

5 Ratner, M. A.; Ratner, D. *Nanotechnology: A Gentle Introduction to the Next Big Idea*; Prentice Hall: New York, 2002.

6 (a) Midgley, P. A.; Ward, E. P. W.; Hungria, A. B.; Thomas, J. M. Nanotomography in the chemical, biological and materials sciences. *Chem. Soc. Rev.* **2007**, *36*, 1477–1494. (b) Midgley, P. A.; Weyland, M.; Thomas, J. M. Electron tomography of nanoparticle catalysts: A new technique based on Rutherford scattering. *J. Phys. Chem. B* **2001**, *105*, 7882–7886.

7 Gabor, D. Microscopy by reconstructed wave-fronts. *Proc. R. Soc London, Ser. A* **1949**, *197*, 454–487.

8 Park, S. J.; Kim, S.; Lee, S.; Khim, Z. G.; Char, K.; Hyeon, T. Synthesis and magnetic studies of uniform iron nanorods and nanospheres. *J. Am. Chem. Soc.* **2000**, *122*, 8581–8582.

9 Puntes, V. F.; Krishnan, K. M.; Alivisatos, A. P. Colloidal nanocrystal shape and size control: The case of cobalt. *Science* **2001**, *291*, 2115–2117.

10 Ould-Ely, T.; Pan, C.; Amiens, C.; Chaudret, B.; Dassenoy, F.; Lecante, P.; Casanove, M.-J.; Mosset, A.; Respaud, M.; Broto, J.-M. Nanoscale bimetallic Co_xPt_{1-x} particles dispersed in poly(vinylpyrrolidone): Synthesis from organometallic precursors and characterization. *J. Phys. Chem. B* **2000**, *104*, 695–702.

11 Tirado, J.-L.; Thomas, J. M.; Jefferson, D. A.; Millward, G. R.; Charles, S. W. On the ultrastructure and morphology of colloidal cobalt ferrite. *J. Chem. Soc., Chem. Commun.* **1987**, 365–368.

12 Ohkoshi, S.-I.; Tokoro, H.; Hozumi, T.; Zhang, Y.; Hashimoto, K.; Mathonière, C.; Bord, I.; Rombaut, G.; Verelst, M.; Cartier dit Moulin, C.; Villain, F. Photo-induced magnetization in copper octacyanomolybdate. *J. Am. Chem. Soc.* **2006**, *128*, 270–277.

13 Ohkoshi, S.-I.; Arai, K. I.; Sato, Y.; Hashimoto, K. Humidity-induced magnetization and pole inversion in a cyano-bridged metal assembly. *Nat. Mater.* **2004**, *3*, 857–861.

14 Dunin-Borkowski, R. E.; McCartney, M. R.; Frankel, R. B.; Bazylinski, D. A.; Pósfai, M.; Buseck, P. R. Magnetic microstructure of magnetotactic bacteria by electron holography. *Science* **1998**, *282*, 1868–1870.

15 Tripp, S. L.; Dunin-Borkowski, R. E.; Wei, A. Flux closure in self-assembled cobalt nanoparticle rings. *Angew. Chem., Int. Ed.* **2003**, *42*, 5591–5593.

16 Price, G. D. Subsolidus phase-relations in the titanomagnetite solid-solution series. *Am. Mineral.* **1981**, *66*, 751–758.

17 Thomas, J. M.; Williams, B. G.; Sparrow, T. G. Electron energy loss spectroscopy and the study of solids. *Acc. Chem. Res.* **1985**, *18*, 324–330.

18 Midgley, P. A.; Weyland, M. A.; Yates, T. J. V.; Arslan, I.; Dunin-Borkowski, R. E.; Thomas, J. M. Nanoscale scanning transmission electron microscopy. *J. Microsc.* **2006**, *223*, 185–190.

19 Dunin-Borkowski, R. E.; Kasama, T.; Harrison, R. J. Electron holography of nanostructured materials. In *Nanocharacterisation*; Kirkland, A. I., Hutchison, J. L., Eds.; Royal Society of Chemistry: London, 2007.

20 Dunin-Borkowski, R. E.; McCartney, M. R.; Smith, D. J. *Electron Holography of Nanostructured Materials*; Nalwa, H. S. Ed.; American Scientific Publishers: Stevenson Ranch, CA, 2004; Vol. 3, pp 41−99.

21 Midgley, P. A. An introduction to off-axis electron holography. *Micron* **2001**, *32*, 167–184.

22 This is an electron-ordering transition, which occurs at approximately 120 K in Fe_3O_4 that is better described as a ferrospinel that is magnetic: $Fe^{3+}(Fe^{3+}Fe^{2+})O_4$. At the Verwey transition, the Fe^{3+} and Fe^{2+} ions order within the octahedral sites.

23 (a) Snoeck, E.; Dunin-Borkowski, R. E.; Dumestre, F.; Renaud, P.; Amiens, C.; Chaudret, B.; Zurcher, P. Quantitative magnetization measurements on nanometer ferromagnetic cobalt wires using electron holography. *Appl. Phys. Lett.* **2003**, *82*, 88–90. (b) Feinberg, J. M.; Harrison, R. J.; Kasama, T.; Dunin-Borkowski, R. E.; Scott, G. R.; Renne, P. R. Effects of internal mineral structures on the magnetic remanence of silicate-hosted titanomagnetite inclusions: An electron holography study. *J. Geophys. Res.* **2006**, *111*, B12S15.

24 (a) Weyland, M. A.; Yates, T. J. V.; Dunin-Borkowski, R. E.; Laffont, L.; Midgley, P. A. Nanoscale analysis of three-dimensional structures by electron tomography. *Scr. Mater.* **2006**, *55*, 29–33. (b) Dunin-Borkowski, R. E.; McCartney, M. R.; Pósfai, M.; Frankel, R. B.; Bazylinski, D. A.; Buseck, P. R. Off-axis electron holography of magnetotactic bacteria: magnetic microstructure of strains MV-1 and MS-1. *Eur. J. Mineral.* **2001**, *13*, 671–684. (c) Simpson, E. T.; Kasama, T.; Posfai, M.; Buseck, P. R.; Harrison, R. J.; Dunin-Borkowski, R. E. Magnetic induction mapping of magnetite chains in magnetotactic bacteria at room temperature and close to the Verwey transition using electron holography. *J. Phys. Conf. Ser.* **2005**, *17*, 108–121.

25 Tripp, S. L.; Pusztay, S. V.; Ribble, A. E.; Wei, A. Self-assembly of cobalt nanoparticle rings. *J. Am. Chem. Soc.* **2002**, *124*, 7914–7915.

26 Tripp, S. L.; Dunin-Borkowski, R. E.; Wei, A. Flux closure in self-assembled cobalt nanoparticle rings. *Angew. Chem., Int. Ed.* **2003**, *42*, 5591–5593.

27 Dunin-Borkowski, R. E.; Kasama, T.; Wei, A.; Tripp, S. L.; Hytch, M. J.; Snoeck, E.; Harrison, R. J.; Putnis, A. Off-axis electron holography of magnetic nanowires and chains, rings and planar arrays of magnetic nanoparticles. *Microsc. Res. Technol.* **2004**, *64*, 390–402.

28 Evans, D. F.; Wennerstrom, H. *The Colloidal Domain: Where Physics, Chemistry, Biology and Technology Meet*, 2nd ed.; Wiley-VCH: New York, 1999.

29 Ramdohr, P. Ulvöspinel and its significance in titaniferous iron ores. *Econ. Geol.* **1953**, *48*, 677–688.

30 Harrison, R. J.; Dunin-Borkowski, R. E.; Putnis, A. Direct imaging of nanoscale magnetic interactions in minerals. *Proc. Natl. Acad. Sci. U.S.A.* **2002**, *99*, 16556–16561.

31 McConnell, J. D. C. Microstructures of minerals as petrogenetic indicators. *Annu. Rev. Earth Planet. Sci.* **1975**, *3*, 125–155.

32 Harrison, R. J.; Dunin-Borkowski, R. E.; Simpson, E. T.; Kasama, T.; McEnroe, S. A. Magnetism and microscopy: applications to mineral magnetism at the nanometer scale. Paper presented at the American Geophysical Union Fall Meeting, San Francisco, 13−17 December 2004.

33 Jourdain, V.; Simpson, E. T.; Paillet, M.; Kasama, T.; Dunin-Borkowski, R. E.; Ponchanal, P.; Zohab, A.; Loiseau, A.; Robertson, J.; Bernier, P. Periodic inclusion of room-temperature ferromagnetic metal phosphide nanoparticles in carbon nanotubes. *J. Phys. Chem. B* **2006**, *110*, 9759–9763.

34 de Ruijter, W. J.; Weiss, J. K. Detection limits in quantitative off-axis electron holography. *Ultramicroscopy* **1993**, *50*, 269–283.

35 (a) Thomas, J. M.; Terasaki, O.; Gai, P. L.; Gonzalez-Calbet, J. M.; Zhou, W. Structural elucidation of microporous and mesoporous catalysts and molecular sieves by high-resolution electron microscopy. *Acc. Chem. Res.* **2001**, *34*, 583–594. (b) Thomas, J. M.; Terasaki, O. The electron microscope is an indispensable instrument for the characterization of catalysts. *Top. Catal.* **2002**, *21*, 155–160.

36 Edwards, P. P.; Thomas, J. M.; Anderson, P. A. Dissolved alkali metals in zeolites. *Acc. Chem. Res.* **1996**, *29*, 23–29.

37 Nozue, Y.; Kodaira, T.; Ohwashi, S.; Goto, T.; Terasaki, O. Ferromagnetic properties of potassium clusters incorporated into zeolite LTA. *Phys. Rev. B* **1993**, *48*, 12253–12261.

38 Caudillo, R.; Gao, X.; Escudero, R.; Jose-Yacaman, M.; Goodenough, J. B. Ferromagnetic behavior of carbon nanospheres encapsulating silver nanoparticles. *Phys. Rev. B* **2006**, *74*, 214418.

39 Coey, J. M. D. Dilute magnetic oxides. *Curr. Opin. Solid State Mater. Sci.* **2006**, *10*, 83–92.

40 The percolation threshold, x_p, is approximately equal to $2/Z$ where Z is the coordination number of the cation. Values of the Z in oxides lie between 4 and 8, so normally x_p is greater than 15%. In the dilute magnetic oxides considered here, the 3d dopant concentration is generally lower than 10%.

41 Coey, J. M. D. d^0 ferromagnetism. *Solid State Sci.* **2005**, *7*, 660–667.

42 Ahmadi, T. S.; Wang, Z. L.; Green, T. C.; El-Sayed, M. A. Shape-controlled synthesis of colloidal platinum nanoparticles. *Science* **1996**, *272*, 1924–1926.

43 Rossi, L. M.; Silva, F. P.; Vono, L. L. R.; Kiyohara, P. K.; Duarti, E. L.; Itri, R.; Landens, R.; Machada, G. Superparamagnetic nanoparticle-supported palladium: a highly stable magnetically recoverable and reusable catalyst for hydrogenation reactions. *Green Chem.* **2007**, *9*, 379–385.

44 Thomas, J. M.; Johnson, B. F. G.; Raja, R.; Sankar, G.; Midgley, P. A. High-performance nanocatalysts for single-step hydrogenations. *Acc. Chem. Res.* **2003**, *36*, 20–30.

45 Thomas, J. M.; Gai, P. L. Electron microscopy and the materials chemistry of solid catalysts. *Adv. Catal.* **2004**, *48*, 171–227.

46 Lobastov, V.; Weissenrieder, J.; Tang, J.; Zewail, A. H. Ultrafast electron microscopy (UEM): Four-dimensional imaging and diffraction of nanostructures during phase transitions. *Nano Lett.* **2007**, *7*, 2552–2558.

47 Chen, J.; Hirayama, T.; Lai, G.; Tanji, T.; Ishizuka, K.; Tonomura, A. Real-time electron-holographic interference microscopy with a liquid crystal spatial light modulator. *Opt. Lett.* **1993**, *18*, 1887–1889.

48 Völkl, E. Live electron holography: Window to the phase world. *Microsc. Microanal.* **2000**, *6*, 211–217.

49 Ciofini, L.; Laine, P. P.; Zamboni, M.; Daul, C. A.; Marvaud, V.; Adamo, C. Intramolecular spin alignment in photomagnetic molecular devices: A theoretical study. *Chem.—Eur. J.* **2007**, *13*, 5360–5377.